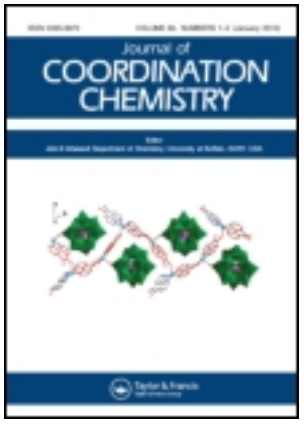

Journal of Coordination Chemistry
Publication details, including instructions for authors and subscription information:
http://www.tandfonline.com/loi/gcoo20

Intermolecular interaction and magnetic coupling mechanism on a mononuclear Co^{II} complex

Shi-Guo Zhang [a], Hong Li [a], Long-Miao Xie [b], Hu Chen [b], Li Yu [b] & Jing-Min Shi [b]

[a] Department of Chemistry and Chemical Engineering, Binzhou Key Laboratory of Material Chemistry, Binzhou University, Binzhou 256603, P.R. China

[b] Department of Chemistry, Shandong Normal University, Jinan 250014, P.R. China

Accepted author version posted online: 04 May 2012.Published online: 22 May 2012.

To cite this article: Shi-Guo Zhang, Hong Li, Long-Miao Xie, Hu Chen, Li Yu & Jing-Min Shi (2012) Intermolecular interaction and magnetic coupling mechanism on a mononuclear Co^{II} complex, Journal of Coordination Chemistry, 65:12, 2211-2220, DOI: 10.1080/00958972.2012.688961

To link to this article: http://dx.doi.org/10.1080/00958972.2012.688961

Journal of Coordination Chemistry
Vol. 65, No. 12, 20 June 2012, 2211–2220

Intermolecular interaction and magnetic coupling mechanism on a mononuclear Co^{II} complex

SHI-GUO ZHANG†, HONG LI†, LONG-MIAO XIE‡, HU CHEN‡, LI YU‡ and JING-MIN SHI*‡

†Department of Chemistry and Chemical Engineering, Binzhou Key Laboratory of Material Chemistry, Binzhou University, Binzhou 256603, P.R. China
‡Department of Chemistry, Shandong Normal University, Jinan 250014, P.R. China

(*Received 8 November 2011; in final form 14 March 2012*)

Anti-ferromagnetic interaction was observed in a new crystal that consists of mononuclear Co^{II} complexes, namely [Co(PMP)(N_3)] (PMP = 2,9-bis(pyridin-2-methoxyl)-1,10-phenanthroline); in the mononuclear complex Co^{II} has a distorted trigonal-bipyramidal geometry. Analysis for the crystal structure indicates six magnetic coupling pathways among adjacent complexes, in which three involve π–π stacking and the other three deal with intermolecular interactions. The fitting for the variable-temperature magnetic susceptibilities with the Curie–Weiss formula shows an anti-ferromagnetic interaction between adjacent Co^{II} ions with $\theta = -5.49$ K $= -3.82\,cm^{-1}$. Theoretical calculations on the spin section reveal that the three π–π stacking systems result in magnetic coupling constants $2J = -0.10\,cm^{-1}$, $-0.10\,cm^{-1}$, and $1.24\,cm^{-1}$, respectively, and the three intermolecular interactions lead to weak anti-ferromagnetic interactions with $2J = -0.36\,cm^{-1}$, $-0.26\,cm^{-1}$, and $-0.32\,cm^{-1}$, respectively. The theoretical calculations and the experimental magnetic data imply that the anti-ferromagnetic interaction involves the orbital contribution of the relevant Co^{II} ions.

Keywords: Crystal structure; Magnetic coupling; π–π Stacking; Cobalt(II) complex; Theoretical calculation; Broken-symmetry theory

1. Introduction

Molecular magnetism has attracted considerable attention with major advances in both their description and their application as new molecular-based materials [1–3]. In magneto-structure correlations it is very important to obtain basic information about magnetic coupling signs, magnitudes, and mechanism. In order to obtain this information many fitting models or fitting formulae have been developed. Theoretical calculations have also been successfully developed for binuclear and trinuclear models to reveal the factors that may dominate the magnetic coupling properties. Mostly, fittings and calculations deal with systems where the coupling spin-carriers (radical or paramagnetic metallic ions) are connected by bridging ligands [4–8] with magnetic interactions through bond exchange. Intermolecular interaction may also

*Corresponding author. Email: shijingmin1955@gmail.com

ISSN 0095-8972 print/ISSN 1029-0389 online
http://dx.doi.org/10.1080/00958972.2012.688961

play an important role in magnetic coupling. For example, some authors attributed strong ferromagnetic order to π–π stacking interaction [9], and other authors found that the π–π stacking interaction led to a strong anti-ferromagnetic interaction between spin carriers [10–12]. Bertrand *et al*. [13] reported strong anti-ferromagnetic interaction between Cu^{II} ions through O–H···O hydrogen-bonding. Thus, intermolecular interactions should be key factors for magnetic coupling properties. However, there is not as much work published on π–π stacking and hydrogen-bond systems as on bond exchange systems, and mostly, they deal with radicals or complexes with radicals as ligands [14–16]. On magnetic coupling signs from π–π stacking, although McConnell I spin-polarization mechanism and McConnell II charge transfer mechanism have been used [17, 18] for some compounds, there are still a few points to be resolved. Factors that dominate the magnetic coupling properties have not been mentioned. Therefore, it is important to design and synthesize complexes with intermolecular interactions and to study the factors that dominate magnetic coupling, an area to which our attention has been given [19–24].

2,9-Bis(pyridin-2-methoxyl)-1,10-phenanthroline (PMP) is an ideal ligand possessing both strong chelating group and larger conjugation plane which may be used to form complexes with strong π–π stacking and relevant magnetic coupling pathway; only one Cu^{II} complex with PMP has been reported [24]. To examine the magnetic coupling mechanism of intermolecular interaction, we synthesize the Co^{II} complex with PMP and report its synthesis and the magnetic coupling mechanism from the intermolecular interaction, which involves both experimental and theoretical calculations.

2. Experimental

2.1. *Materials*

PMP was synthesized through the reaction of 2,9-dichloro-1,10-phenanthroline and (pyridine-2-yl)methanol [24]; all other chemicals are of analytical grade and used without further purification.

2.2. *[Co(PMP)(N_3)$_2$]*

Methanol solution (10 mL) of PMP (0.0527 g, 1.34×10^{-4} mol) was added to 5 mL water solution containing $Co(ClO_4)_2 \cdot 6H_2O$ (0.0570 g, 1.56×10^{-4} mol) and 5 mL NaN_3 (0.0313 g, 4.81×10^{-4} mol) and stirred for a few minutes. Red single crystals were obtained after the filtrate was allowed to slowly evaporate at room temperature for 2 weeks. IR (cm^{-1}): 2054(s), 1602(s), 1565(m), 1499(s), 1313(s), 1054(m), 1008(m). Elemental anal. Calcd for $C_{24}H_{18}CoN_{10}O_2$: (fw 537.41) C, 53.64; H, 3.38; N, 26.07; Co, 10.97. Found (%): C, 53.43; H, 3.67; N, 26.45; Co, 11.45.

2.3. *Physical measurements*

Infrared spectrum was recorded with a Bruker Tensor 27 infrared spectrometer from 4000 cm^{-1} to 500 cm^{-1} using KBr disc. C, H, and N elemental analyses were carried out

on a Perkin-Elmer 240 instrument. Variable-temperature magnetic susceptibilities of microcrystalline powder sample were measured in a magnetic field of 1 kOe from 2.00 K to 300 K on a SQUID magnetometer. The data were corrected for magnetization of the sample holder and for diamagnetic contributions of the complex which were estimated from Pascal's constants.

2.4. *Computational details*

The magnetic interactions between Co^{II} ions were studied by density functional theory coupling with the broken-symmetry approach [25–27]. Exchange coupling constants J have been evaluated by calculating the energy difference between the high-spin state (E_{HS}) and the broken symmetry state (E_{BS}), assuming the spin Hamiltonian is defined as

$$\hat{H} = -2J\hat{S}_1 \cdot \hat{S}_2 \tag{1}$$

If the spin projected approach is used, the equation proposed by Noodleman [25–27] to extract the J-value for a binuclear transition-metal complex is thus:

$$J = \frac{E_{BS} - E_{HS}}{4S_1S_2} \tag{2}$$

To obtain exchange coupling constants J, Orca 2.8.0 calculations [28] were performed with the popular spin-unrestricted hybrid functional B3LYP proposed by Becke [29, 30] and Lee *et al*. [31], which can provide J-values in agreement with the experimental data for transition metal complexes [32, 33]. Tri-ζ with one polarization function def2-TZVP [34, 35] basis set proposed by Ahlrichs and co-workers for all atoms was used in our calculations. Strong convergence criteria were used to ensure that the results are well converged with respect to technical parameters (the system energy was set to be smaller than 10^{-7} Hartree).

2.5. *X-ray crystallographic determination of the complex*

A red single crystal of dimensions $0.53 \times 0.32 \times 0.13\,mm^3$ was selected and subsequently glued to the tip of a glass fiber. Determination of the crystal structure at 25°C was carried out on an X-ray diffractometer (Bruker Smart-1000 CCD) using graphite monochromated Mo-Kα radiation ($\lambda = 0.71073$ Å). Corrections for L_p factors were applied and all non-hydrogen atoms were refined with anisotropic thermal parameters. Hydrogen atoms were placed in calculated positions and refined as riding. The programs for structure solution and refinement were SHELXS-97 and SHELXL-97, respectively [36–38]. The pertinent crystallographic data and structural refinement parameters are summarized in table 1.

3. Results and discussion

3.1. *Crystal structure of [Co(PMP)(N_3)$_2$]*

Figure 1 shows the coordination diagram with the atom-numbering scheme and table 2 gives the coordination bond lengths and associated angles. The coordination bond

Table 1. Crystal data and structure refinement for the complex.

Formula	$C_{24}H_{18}CoN_{10}O_2$
Formula weight	537.41
Temperature (K)	298
Crystal system	Triclinic
Space group	$P\bar{1}$
Unit cell dimensions (Å, °)	
a	8.8405(15)
b	10.5857(18)
c	13.725(2)
α	73.129(2)
β	81.284(2)
γ	68.196(2)
Volume (Å^3), Z	1139.8(3), 2
Calculated density (g cm^{-1})	1.566
Absorption coefficient (mm^{-1})	0.800
Reflections collected	6229
Independent reflection	4375
Goodness-of-fit on F^2	1.055
R_1 [$I > 2\sigma(I)$]	0.0444
wR_2 (all data)	0.1210
Largest difference peak and hole (e Å^{-3})	0.414 and −0.253

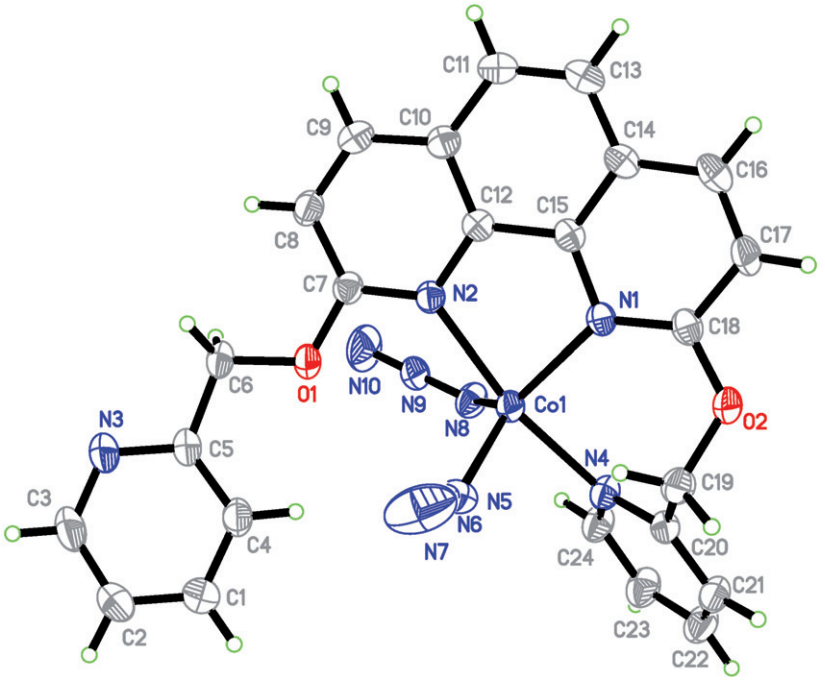

Figure 1. Coordination diagram of the title complex with atom-numbering scheme.

lengths range from 1.980(3) Å to 2.177(3) Å and the associated angles change from 77.10(9)° to 168.31(9)°. Co1 assumes a distorted trigonal-bipyramidal geometry due to its Addison constant [39] $\tau = (\beta - \alpha)/60 = 0.69$. The non-hydrogen atoms of 1,10-phenanthroline define an approximate plane within 0.0202 Å with a maximum

Table 2. Selected bond lengths (Å) and angles (°).

Co1–N8	1.978(2)	Co1–N5	1.994(3)	Co1–N1	2.156(2)
Co1–N4	2.173(2)	Co1–N2	2.175(2)		
N8–Co1–N5	117.65(11)	N8–Co1–N1	126.71(9)	N5–Co1–N1	115.47(10)
N8–Co1–N4	87.78(9)	N5–Co1–N4	91.62(10)	N1–Co1–N4	
N8–Co1–N2	90.11(8)	N5–Co1–N2	99.58(9)	N1–Co1–N2	94.86(8)
N4–Co1–N2	168.25(8)				77.18(8)

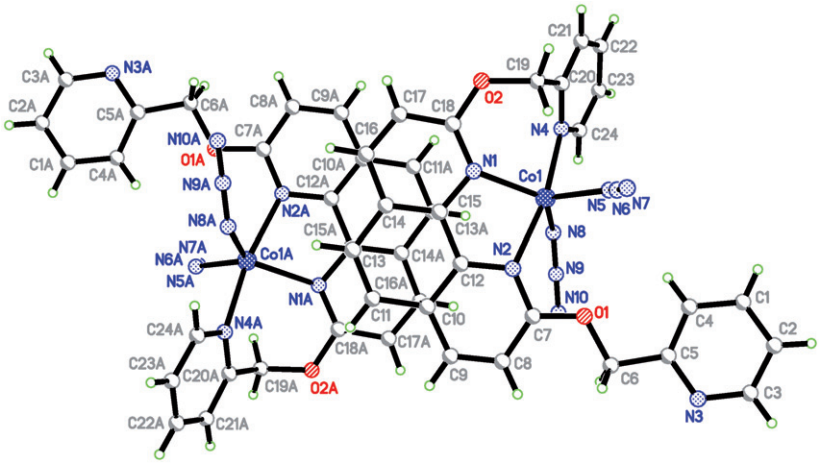

Figure 2. The π–π stacking between adjacent complexes with PS-1 and Model 1 (symmetry code: $1-x$, $1-y$, $-z$).

deviation of –0.0496(24) for C18. In the crystal there are three π–π stacking interactions [40] among adjacent complexes as shown in figure 2 with the name PS-1, figure 3 with the name PS-2, and figure 4 with the name PS-3, respectively. Both PS-1 and PS-2 involve symmetry-related 1,10-phenanthroline rings slipped π–π stacking, whereas PS-3 deals with symmetry-related pyridine rings slipped π–π stacking. The relevant slipped π–π stacking interplanar distances of PS-1, PS-2, and PS-3 are 3.373 Å, 3.440 Å, and 3.138 Å (3.45 Å as accepted maximum distance for a π–π stacking), respectively. Relevant non-bonded atoms' separation distances of the three π–π stacking systems are C10 · · · C16A (or C16 · · · C10A), 3.374(4) Å; C13 · · · C15A (or C15 · · · C13A) 3.395(4) Å; Co1 · · · Co1A, 8.2402(11) Å (symmetry code: $1-x$, $1-y$, $-z$) for PS-1; C7 · · · C10A (or C10 · · · C7A), 3.494(4) Å; C9 · · · C12A (or C12 · · · C9A), 3.493(4) Å; Co1 · · · Co1A, 8.6994(13) Å (symmetry code: $-x$, $1-y$, $-z$) for PS-2 and C23 · · · C24A (or C24 · · · C23A), 3.458(5) Å; Co1 · · · Co1A, 7.7764(11) Å (symmetry code: $1-x$, $-y$, $1-z$) for PS-3. In the crystal, there are three other pairs of adjacent complexes with Co · · · Co distances of 8.8405(15) Å with the name IM-1, 8.9755(12) Å with the name IM-2, and 8.8405(15) Å with the name IM-3, respectively. These separation distances are very close to those of the π–π systems mentioned above. Therefore, magnetic couplings may exist in each pair of complexes.

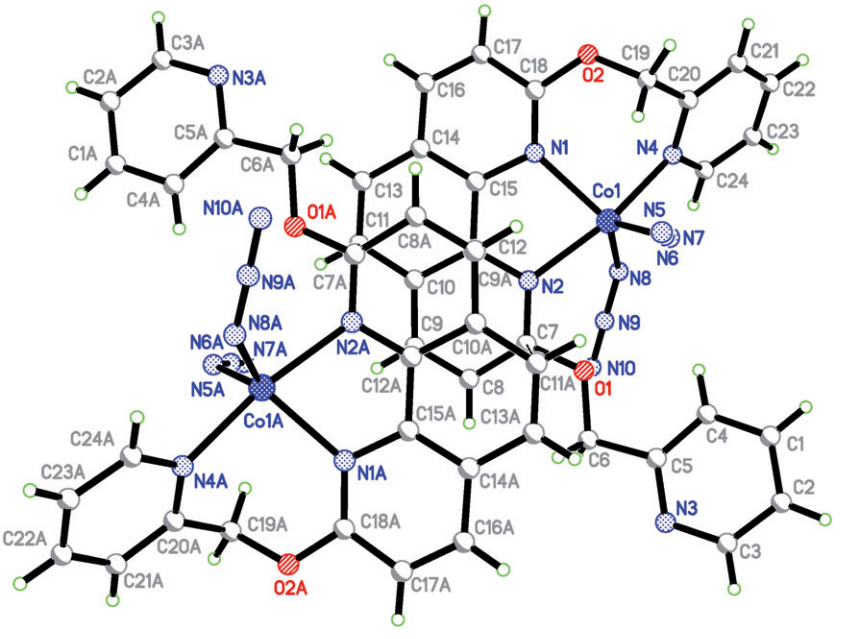

Figure 3. The π–π stacking between adjacent complexes with PS-2 and Model 2 (symmetry code: $-x, 1-y, -z$).

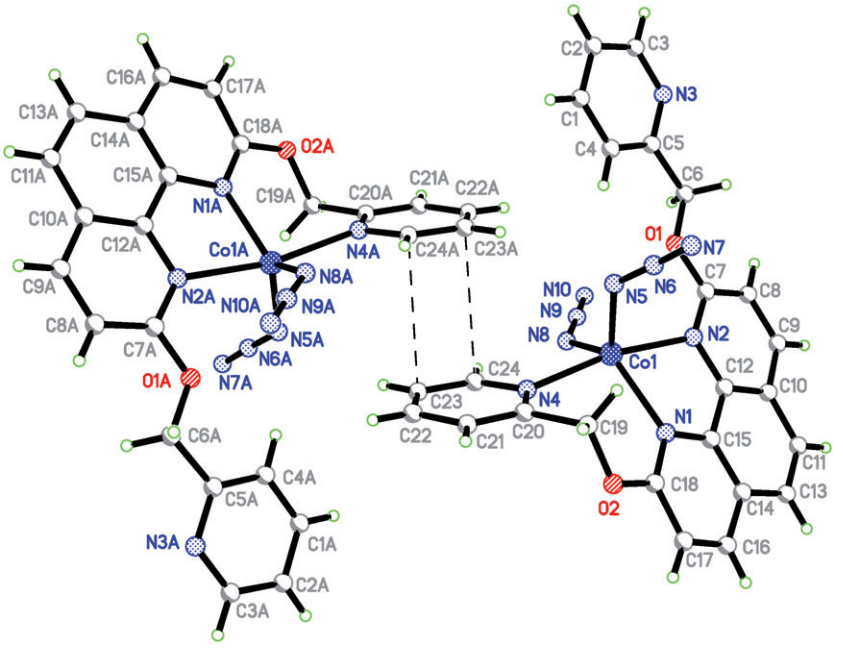

Figure 4. The π–π stacking between adjacent complexes with PS-3 and Model 3 (symmetry code: $1-x, -y, 1-z$).

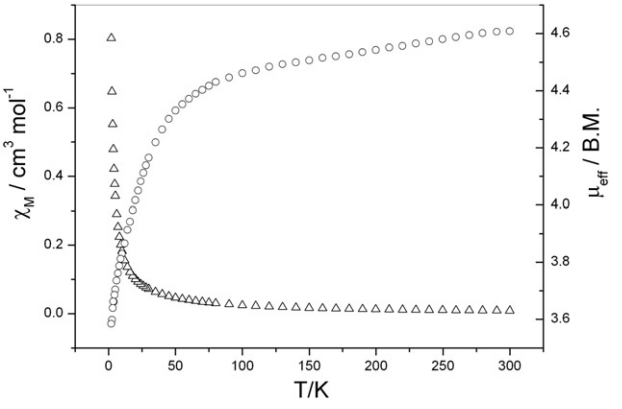

Figure 5. Plots of χ_M (the open triangle for the experimental data) and μ_{eff} (the open circle for the experimental data) *vs.* T for the complex.

3.2. *Magnetic studies*

3.2.1. Experimental data fitting results. The variable-temperature (2.00–300 K) magnetic susceptibilities are shown in figure 5, where χ_M is the molar magnetic susceptibility per Co^{II} and μ_{eff} is the magnetic moment per Co^{II}. Figure 5 shows that the χ_M value increases with decreasing temperature, reaching a maximum at 2.00 K. The μ_{eff} at 300 K is 4.61 B.M., larger than the value expected for an isolated spin-only (3.87 B.M., $g_{av} = 2$) at room temperature, indicating an important orbital contribution is involved [41]. The μ_{eff} value decreases very slowly with temperature drop until about 80.0 K, and then μ_{eff} decreases sharply with temperature drop and reaches 3.58 B.M. at 2.00 K, which suggests that there is an anti-ferromagnetic interaction between adjacent Co^{II} ions. The χ^{-1} *versus* T plot follows the Curie–Weiss law with $C = 2.67\,cm^3\,mol^{-1}\,K$ and $\theta = -5.49\,K = -3.82\,cm^{-1}$ as shown in figure 6, which further indicates that there is a weak anti-ferromagnetic interaction between adjacent Co^{II} complexes. To understand the magnetic coupling mechanism from the spin theoretical calculations were performed.

3.2.2. Theoretical study on magnetic interaction. Density function calculations were based on Models 1–6, as shown in figure 2, figure 3, figure 4, SI-figure 1, SI-figure 2, and SI-figure 3, respectively, in which the former three models stand for PS-1, PS-2, and PS-3 π–π stacking, respectively, and the latter three models for IM-1, IM-2, and IM-3 intermolecular interaction, respectively. The calculations were constrained by the data of bond lengths, associated angles, and relevant locations of adjacent complexes from the X-ray structure. According to equation (2), the calculations gave $2J$-values of $-0.10\,cm^{-1}$, $-0.10\,cm^{-1}$, $1.24\,cm^{-1}$, $-0.36\,cm^{-1}$, $-0.26\,cm^{-1}$, and $-0.32\,cm^{-1}$ for Models 1–6, respectively. PS-3 π–π stacking magnetic coupling pathway functions as a ferromagnetic interaction, whereas the other five magnetic coupling pathways are anti-ferromagnetic interactions, and the anti-ferromagnetic interactions and ferromagnetic interaction should offset each other. The calculated magnetic coupling constants also

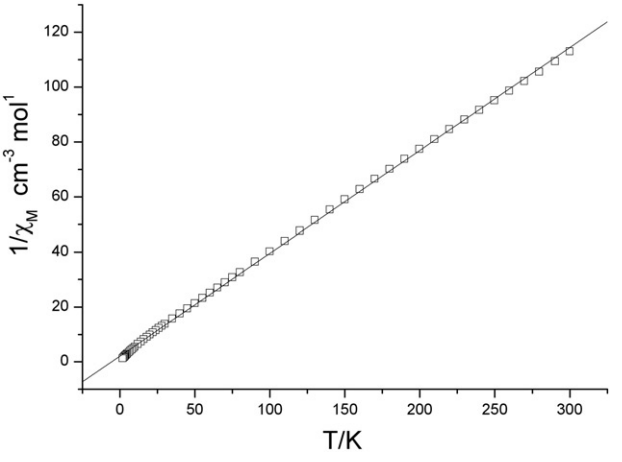

Figure 6. Thermal variation of the reciprocal susceptibility (open square for experimental data).

indicate that these magnetic interactions are not from dipole–dipole interactions of Co^{II} ions.

On magnetic coupling, the sign of π–π stacking McConnell I spin-polarization mechanism [17] has been used to explain the ferromagnetic interaction of $[Mn(Cp^*)_2]^+[Ni(dmit)_2]^-$ complex [42], and McConnell I spin-polarization mechanism considers that a global ferromagnetic interaction arises from interaction between spin densities of opposite sign being predominant, whereas an anti-ferromagnetic interaction results from dominant interaction between spin densities of the same sign. SI-table 1 and SI-figure 4 display the spin density population of the ground state of Model 1. From SI-table 1, the absolute value of the spin density population of each Co^{II} is smaller than 3 and the coordinated nitrogen atoms, except N8 and N8A, exhibit the same sign as the Co^{II} ions, suggesting spin delocalization from the two Co^{II} 3d orbitals to these coordinated nitrogen atoms. Opposite spin densities not only appear on N8 and N8A, but also on a few N and C, which means that there also exists spin polarization phenomenon in this system. Both spin delocalization and spin polarization may benefit the magnetic interaction through the π–π stacking pathway. In Model 1, each pair of atoms exhibits different spin density interaction, and obviously, McConnell I spin polarization mechanism is unable to explain the anti-ferromagnetic interaction mechanism; a similar example has also been reported on a Cu^{II} complex [23].

SI-table 2 and SI-figure 5 reveal the spin density population of the ground state of Model 2, and just as for Model 1 spin delocalization also occurs in Model 2 from the Co^{II} to the associated atoms and at the same time there also exists spin polarization in Model 2. In the π–π stacking system, the pair number of the atoms with the same spin density interaction (C7$\cdots$C10A and C10$\cdots$C7A) equals the pair number of atoms with different spin density interaction (C9$\cdots$C12A and C12$\cdots$C9A), and the distances between the pairs with the same spin density interaction are not smaller than that of the different spin density interaction, and still, the spin densities on atoms with the same spin density interaction are clearly smaller than that of the different spin density interaction. Therefore, the anti-ferromagnetic interaction is hard to explain in terms of McConnell I spin-polarization mechanism in the present situation.

SI-table 3 and SI-figure 6 show the spin density population of the ground state of Model 3, and just as Models 1 and 2 there also exist both spin delocalization and spin polarization in Model 3. In the π–π stacking system two pairs of atoms display the same spin density interaction, indicating that the present ferromagnetic interaction is also hard to explain in terms of McConnell I spin-polarization mechanism. Obviously it is a challenge to explain the present magnetic coupling phenomena.

SI-table 4, SI-table 5, and SI-table 6 display the spin density population of the ground state of Model 4, Model 5, and Model 6, respectively, and from these data it is known that both spin delocalization and spin polarization also occur in the three systems. But the correlation between the spin density and the magnetic coupling strengths or magnetic coupling sign is hard to obtain at present.

The theoretical calculations further confirm that the experimental anti-ferromagnetic interaction involves the orbital contribution of the relevant Co^{II} ions.

4. Conclusion

A new mononuclear Co^{II} complex with PMP as ligand has been synthesized and its crystal structure has been determined, displaying that there are six magnetic coupling pathways. The experimental fitting for variable-temperature magnetic susceptibility data with the Curie–Weiss formula reveals that there is a weak anti-ferromagnetic interaction between adjacent Co^{II} ions. The theoretical calculations on the spin reveal that one of the magnetic coupling pathways resulted in a weak ferromagnetic interaction and other five magnetic coupling pathways led to weak anti-ferromagnetic interactions. The weak anti-ferromagnetic interaction from the experimental fitting should be attributed to both the spin magnetic interaction and the orbital magnetic interaction.

Supplementary material

CCDC 810674 contains detailed information of the Crystallographic data for this article, and these data can be obtained free of charge from the Cambridge Crystallographic Data Centre *via* http://www.ccdc.cam.ac.uk/data_request/cif. SI-figures 1–6 and SI-tables 1–6 can be obtained free of charge from the corresponding author of this journal.

Acknowledgments

This work was supported by the National Natural Science Foundation of China (Grant No. 20971080) and the Natural Science Foundation of Shandong Province (Grant Nos ZR2009BM026 and ZR2009BL002).

References

[1] J.R. Friedman, M.P. Sarachik, J. Tejada, R. Ziolo. *Phys. Rev. Lett*., **76**, 3830 (1996).
[2] G.L.J.A. Rickken, E. Raupack. *Nature*, **405**, 932 (2000).
[3] S. Tanase, J. Reedijk. *Coord. Chem. Rev*., **250**, 2501 (2006).
[4] H. Li, T.-T. Sun, S.-G. Zhang, J.-M. Shi. *J. Coord. Chem*., **63**, 1531 (2010).
[5] C. Wang, J. Li, Y.-W. Ren, F.-G. He, G. Meke, F.-X. Zhang. *J. Coord. Chem*., **61**, 4033 (2008).
[6] H. Li, C. Hou, J.-M. Shi, S.-G. Zhang. *J. Coord. Chem*., **61**, 3501 (2008).
[7] J.-M. Li, X. Jin. *J. Coord. Chem*., **62**, 2610 (2009).
[8] J.-M. Shi, Q.S. Liu, W. Shi. *J. Coord. Chem*., **62**, 1121 (2009).
[9] L.-L. Li, K.-J. Lin, C.-J. Ho, C.-P. Sun, H.-D. Yang. *Chem. Commun*., 1286 (2006).
[10] N.P. Gritsan, A.V. Lonchakov, E. Lork, R. Mews, E.A. Pritchina, A.V. Zibarev. *Eur. J. Inorg. Chem*., 1994 (2008).
[11] K. Goto, T. Kubo, K. Yamanoto, K. Nakasuji, K. Sato, D. Shiomi, T. Takui, M. Kubota, T. Kobayashi, K. Yakusi, J. Ouyang. *J. Am. Chem. Soc*., **121**, 1619 (1999).
[12] B.D. Koivisto, A.S. Ichimura, R. McDonald, M.T. Lemaire, L.K. Thompson, R.G. Hicks. *J. Am. Chem. Soc*., **128**, 690 (2006).
[13] J.A. Bertrand, T.D. Black, P.G. Eller, F.T. Helm, R. Mahmood. *Inorg. Chem*., **15**, 2965 (1976).
[14] L. Norel, F. Pointillart, C. Train, L.-M. Chamoreau, K. Boubekeur, Y. Journaux, A. Brieger, D.J.R. Brook. *Inorg. Chem*., **47**, 2396 (2008).
[15] X.M. Ren, S. Nishihara, T. Akutagawa, S. Noro, T. Nakamura. *Inorg. Chem*., **45**, 2229 (2006).
[16] R.K. Kremer, B. Kanellakopulos, P. Bele, H. Brunner, F.A. Neugebauer. *Chem. Phys. Lett*., **230**, 255 (1994).
[17] K. Yoshizawa, R. Hoffmann. *J. Am. Chem. Soc*., **117**, 6921 (1995).
[18] J.S. Miller, A.J. Epstein. *J. Am. Chem. Soc*., **109**, 3850 (1987).
[19] H. Li, S.-G. Zhang, L.M. Xie, L. Yu, J.-M. Shi. *J. Coord. Chem*., **64**, 1456 (2011).
[20] J.-M. Shi, X.-Z. Meng, Y.-M. Sun, H.-Y. Xu, W. Shi, P. Cheng, L.-D. Liu. *J. Mol. Struct*., **917**, 164 (2009).
[21] L. Yu, J.-M. Shi, Y.-Q. Zhang, Y.-Q. Wang, Y.-N. Fan, G.-Q. Zhang, W. Shi, P. Cheng. *J. Mol. Struct*., **987**, 138 (2011).
[22] C. Hou, J.-M. Shi, Y.-M. Sun, W. Shi, P. Cheng, L.-D. Liu. *Dalton Trans*., **37**, 5970 (2008).
[23] Y.-H. Chi, L. Yu, J.-M. Shi, Y.-Q. Zhang, T.Q. Hu, G.Q. Zhang, W. Shi, P. Cheng. *Dalton Trans*., **40**, 1453 (2011).
[24] H. Li, S.-G. Zhang, L.-M. Xie, L. Yu, J.-M. Shi. *J. Coord. Chem*., **64**, 3595 (2011).
[25] L. Noodleman. *J. Chem. Phys*., **74**, 5737 (1981).
[26] L. Noodleman, E.J. Baerends. *J. Am. Chem. Soc*., **106**, 2316 (1984).
[27] L. Noodleman, D.A. Case. *Adv. Inorg. Chem*., **38**, 423 (1992).
[28] F. Neese. *An Ab Initio, DFT and Semiempirical Electronic Structure Package, Program* (*Version 2.7*), Revision 0, Lehrstuhl fuer Theoretische Chemie Institut fuer Physikalische und Theoretische Chemie, Universitaet Bonn, Germany (2010).
[29] A.D. Becke. *J. Chem. Phys*., **98**, 5648 (1993).
[30] A.D. Becke. *Phys. Rev. A*, **38**, 3098 (1988).
[31] C. Lee, W. Yang, R.G. Parr. *Phys. Rev. B*, **37**, 785 (1988).
[32] J. Cano, E. Ruiz, S. Alvarez, M. Verdaguer. *Comments Inorg. Chem*., **20**, 27 (1998).
[33] E. Ruiz, P. Alemany, S. Alvarez, J. Cano. *J. Am. Chem. Soc*., **119**, 1297 (1997).
[34] A. Schaefer, H. Horn, R. Ahlrichs. *J. Chem. Phys*., **97**, 2571 (1992).
[35] F. Weigend, R. Ahlrichs. *Phys. Chem. Chem. Phys*., **7**, 3297 (2005).
[36] G.M. Sheldrick. *Acta Cryst*., **A64**, 112 (2008).
[37] G.M. Sheldrick. *Acta Cryst*., **D66**, 479 (2010).
[38] G.M. Sheldrick. *Acta Cryst*., **A46**, 467 (1990).
[39] A.W. Addison, T.N. Rao, J. Reedjik, J. Van Rijn, C.G. Verschoor. *J. Chem. Soc., Dalton Trans*., 1349 (1984).
[40] C. Janiak. *J. Chem. Soc., Dalton Trans*., 3885 (2000).
[41] H.-L. Sun, Z.M. Wang, S. Gao. *Chem. Eur. J*., **15**, 1757 (2009).
[42] C. Faulmann, E. Riviere, S. Dorbes, F. Senocq, E. Coronado, P. Cassoux. *Eur. J. Inorg. Chem*., 2880 (2003).